Chapter 14

Mechanical Properties of the Thermal Barrier Coatings Made of Cobalt Alloy MAR-M509

Zenon Aleksander Opiekun

Additional information is available at the end of the chapter

http://dx.doi.org/10.5772/61100

Abstract

This manuscript presents the microstructure, geometrical product specification, and results of scratch tests performed on the interlayer of thermal barrier coating (TBC) with Rockwell's intender. The TBC was provided by depositing two layers, metallic interlayer and external ceramic layer, onto a plate coating made of cobalt alloy MAR-M509 in plasma spraying process.

Based on measurements of microhardness made with Berkovitz's indenter using Nano Scratch-Tester (CSM Instruments), it was stated that elastic (Ee) to total energy (Ec) parameters (M_{IT} = Ee/Ec), γ phase matrix of alloy MAR-M509 ($M_{IT\gamma}$), metallic interlayer (45% Ni–22% Co–17% Cr–16% Al–0.3% Y) (M_{ITM}), and ceramic layer (M_{ITZrO2}), are proportion, that is, 0.29:0.22:0.50. The surface of the casting was sandblasted with Al_2O_3 powder in an air stream before the TBC was introduced. Scratches were made along the cross section from a mould material (MAR-M509) through metallic interlayer and external ceramic layer in the TBC. Friction force, friction factor, and acoustic emission were recorded during the test. It has been proven that metallic interlayer in the TBC of ca. 200 μm thickness forms tough coating without pores with good cohesion values and very good adhesion values to the mould.

Keywords: Cobalt alloy MAR-M509, geometrical product specification (GPS), thermal barrier coating (TBC), microstructure, microhardness, interlayer cohesion, adhesion, nanoscratch test

1. Introduction

Thermal barrier coatings (TBCs) are applied via plasma spraying technology (air plasma system [APS]) and build up usually with two layers: metallic interlayer and external ceramic layer [1–3]. For special purposes, when a high density of coating together with its good bonding with the mould is demanded, the TBC is applied in vacuum plasma spraying process (vacuum plasma spray [VPS]) or low-pressure plasma spraying technique (low-pressure plasma spray [LPPS]) [4]. The TBC has an excellent heat resistance and a small thermal conductivity. They are characterized by an erosion and abrasion resistance and resistance to aggressive chemicals [5]. Therefore, TBCs are becoming more commonly used as coatings of jet-propelled parts of aircraft engines (combustor, blade outer air seal [BOAS], and blades of turbine), valves, and parts in chemical reactors [6–7].

Materials with MeCrAlY group single oxides that belong to ceramic materials are usually applied on metallic interlayers. These are most often used on the external layer in the TBC: Al_2O_3, ZrO_2, ThO_2, BeO, MgO, CeO_2, Cr_2O_3i Y_2O_3 [5,6]. Thermal barrier coatings are the layers that separate the surface of metallic material from the stream of hot gases. Simultaneously, they reduce the temperature of metallic items [8]. In the end, such an influence of the TBC causes an improvement of performance characteristic of jet turbine engine, a reduction of fuel consumption, an increase of inlet gas temperature (ca. 100–170°C) (Fig. 1) [9], and a decrease of toxic substance emission from outlet gases because of better fuel consumption [7].

ZrO_2 oxide stabilized by Y_2O_3 is most often used for the external layer in the TBC [10–15]. Functional properties, adhesion, cohesion, and crack resistance depend on the phase composition of this oxide. Solid solutions prepared on the basis of regular ZrO_2 (C) have low resistant to changeable heat load. A considerable improvement of the crack resistance of these solutions is noticed during the presence of tetragonal phase of ZrO_2 (T) in the TBC. Factors that favor the tetragonal phase in the TBC after cooling down to the room temperature from the temperature of plasma spraying are small ZrO_2–8% Y_2O_3 irregular grain sizes, with the introduction of about 8 wt% of Y_2O_3 to the solid solution of ZrO_2–Y_2O_3(Fig. 2) [16].

The aim of this article was to describing the cohesion and adhesion of the metallic interlayer made of 45% Ni–22% Co–17% Cr–16% Al–0.3% Y alloy and to present the geometrical product specification of the ceramic external layer made of ZrO_2 oxides deposited on the casting of plate made of MAR-M509 cobalt alloy.

The main criterion to accommodate metallic interlayer is to compensate stress between the substrate and the external ceramic layer. TBC with plastic interlayer decreases its own stress and enhances connection between harder substrate and fragile hard external ceramic layer [17–19]. Useful properties of TBC (erosion invulnerability, thermal fatigue, scale off, and mastication) depend on fat of layers and their spraying thermal parameters [20–23].

The mechanical properties of TBC layers defined were by microhardness made with Berkovitz's indenter when Nano Scratch-Tester (CSM Instruments) was used. The coating was obtained by single-spraying metallic powder made of 45% Ni–22% Co–17% Cr–16% Al–0.3%

http://dx.doi.org/10.5772/61100

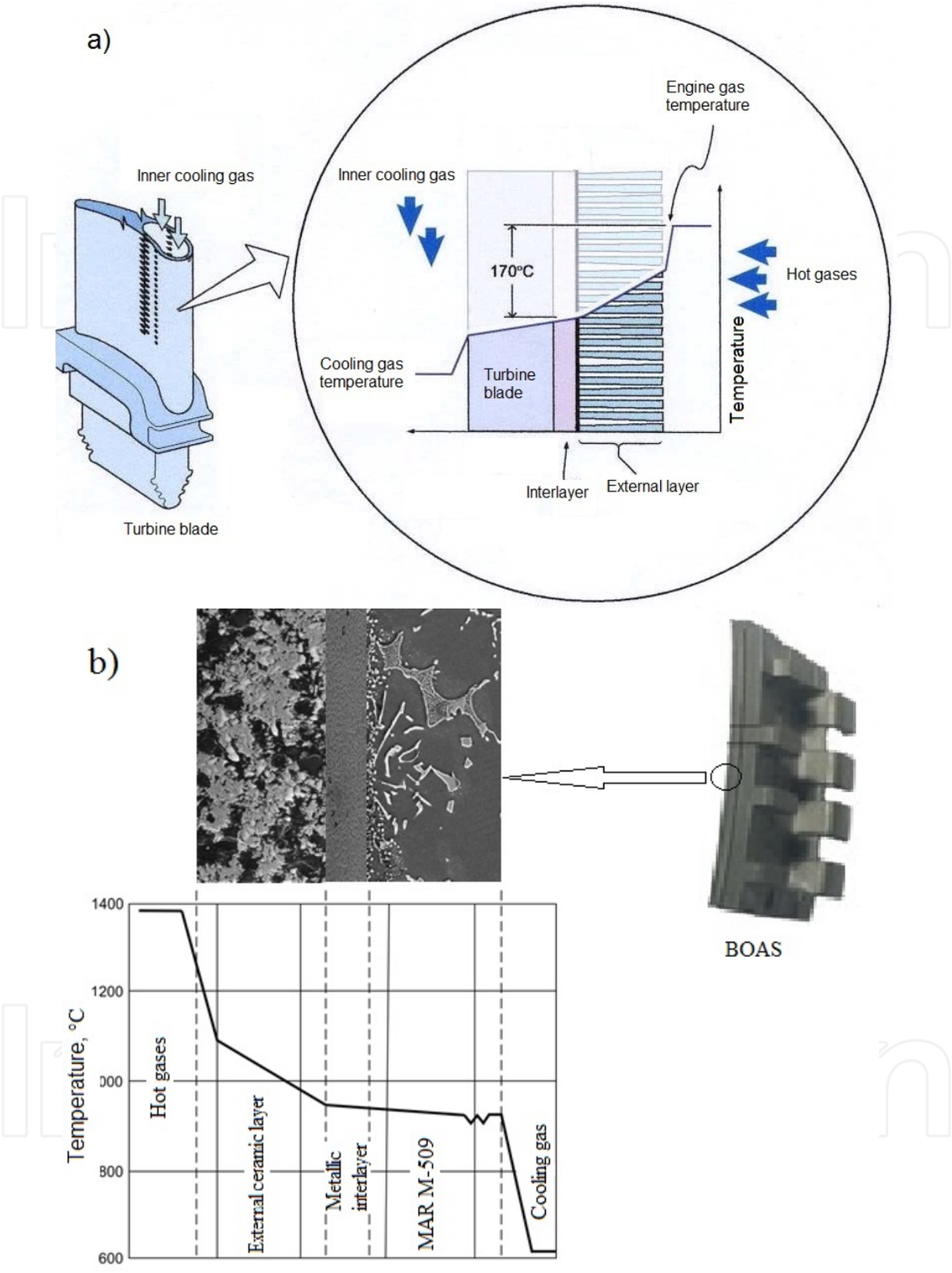

Figure 1. Effect of TBC on reducing temperature of turbine blade [9] (a), and BOAS made of MAR-M509 alloy (b) (schemes).

Y alloy and triple-spraying ceramic powder made of ZrO_2–8% Y_2O_3 oxides onto the surface of the casting with a MultiCoat Plasma Coating System (SulzerMetco).

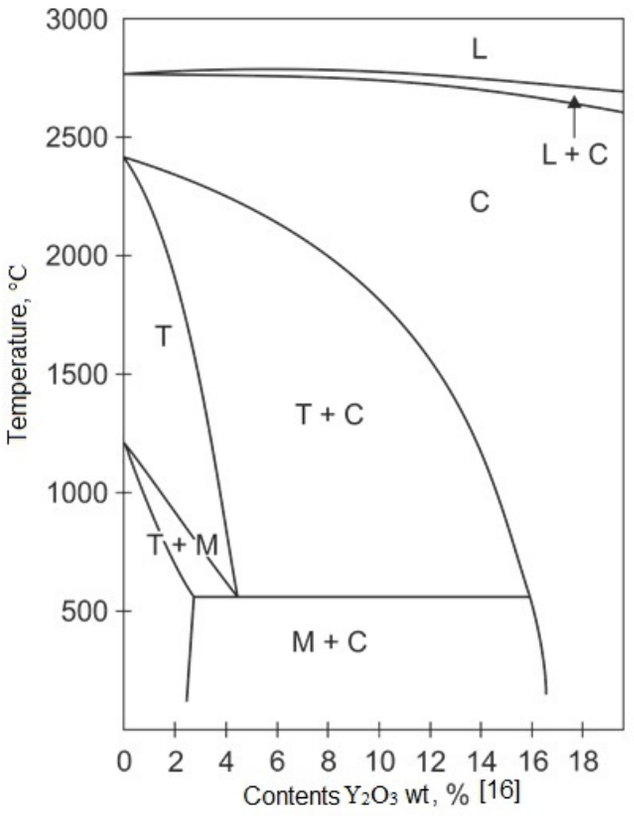

Figure 2. Phase equilibrium system ZrO_2–Y_2O_3.

2. Materials and methods of testing

Plate castings made of cobalt alloy MAR-M509 with a dimension of 4 × 20 × 90 mm were used for tests. The composition of plates was as follows: 0.60% C, 28.83% Cr, 10.0% Ni, 7.12% W, 3.77% Ta, 0.36% Zr, 0.18% Ti, 0.007% B, 0.43% Fe, 0.02% Mn, 0.03% Si, 0.002% S, and the rest is Co. The plates were casted in the multilayer ceramic mould (MCM) at initial temperature ca. 1000°C. The liquid alloy MAR-M509 at temperature ca. 1495 ± 5°C [24,25] was poured over MCM in a medium-frequency induction vacuum furnace. The surface of plate castings was at first sandblasted with Al_2O_3 powder of 200 ÷ 250 μm grain diameter in an air stream of pressure of ca. 0.35 MPa for a few seconds. After a single layer of 45% Ni–22% Co–17% Cr–16% Al–0.3% Y powder alloy was covered, triple layers of ZrO_2–8% Y_2O_3 powder oxides in an argon-hydrogen plasma beam were applied. The plates were heated at a temperature of about 120°C before the layers were covered.

Two spray powders were used in the experiment: one 45% Ni–22% Co–17% Cr–16% Al–0.3% Y powder alloy, which shows fine spherical morphology with particle granulation, ca.75 ± 15 μm, and ZrO_2–Y_2O_3 oxide powder, which shows irregular morphology with particle granulation, ca.53 ± 15 μm.

A deposition of all layers in the TBC was done using the following: primary plasma gas, Ar (40 l/ min); secondary plasma gas, H_2 (10 l/min); electric current, about 600 A; powder feet rate

(40 g/min); and spray distance, about 130 mm. The traverse speed of a spraying gun was constant at 2 mm/min, and the speed of rotating holder was also constant (60 rot/min) (Fig. 3).

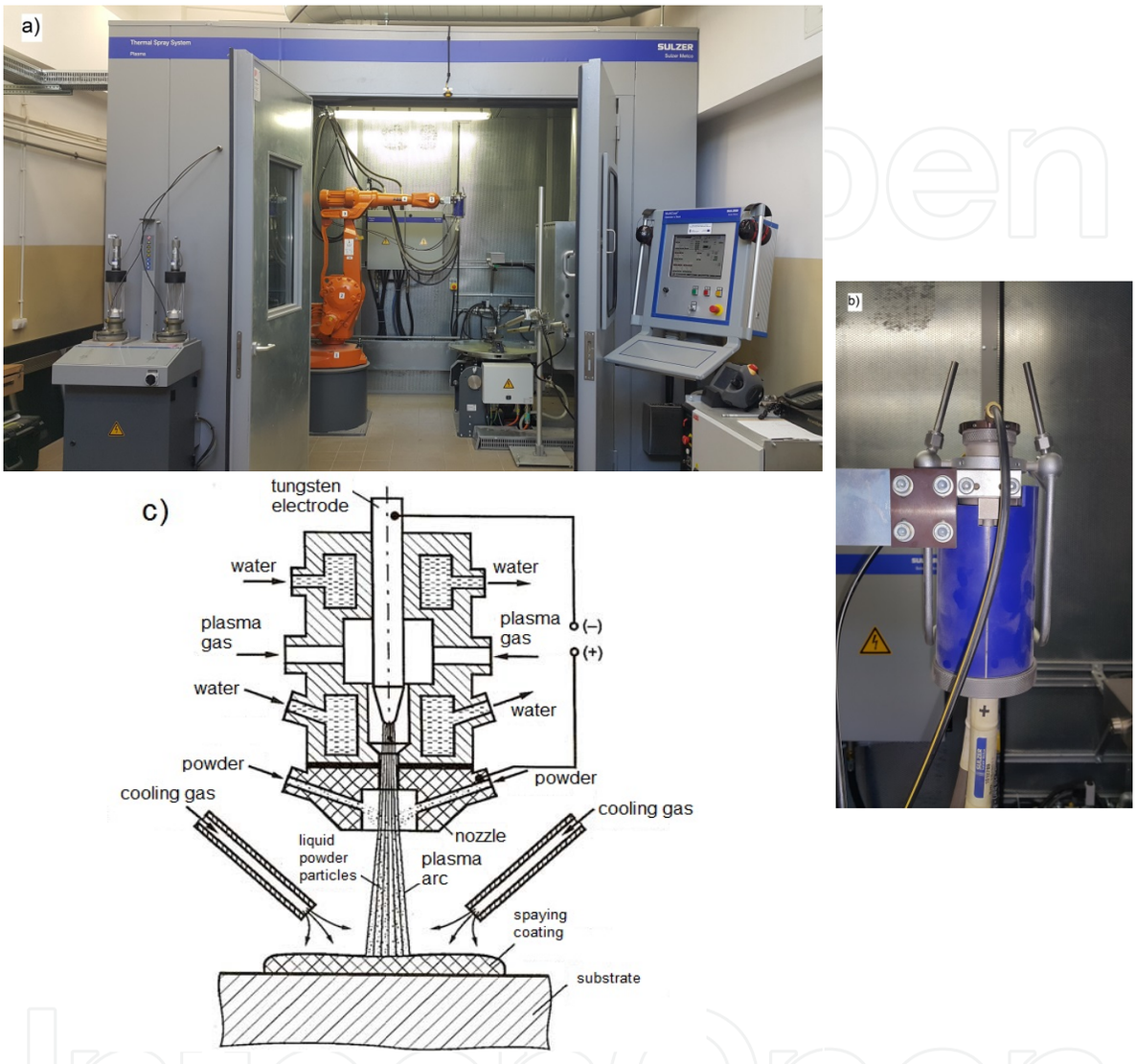

Figure 3. Multicoat plasma coating system. View of system (a), spraying gun F4 MB-HBS type (b), scheme of spraying (c).

The state of surface of plate castings was assessed with the Talyscan 150 (Taylor-Hobson) tool working with the Mountains Map Universal program before and after the ceramic layers was deposited. Six amplitude parameters of geometrical product specification (GPS) were analyzed: S_a (arithmetic mean), S_z (mean of the 5 highest peaks and the 5 lowest points), S_t (total height), S_q (quadratic mean), S_p (highest peak over the mean), and S_v (lowest valley under the mean).

X-ray examination surface of the TBC was performed with the Siemens Kristalloflex D500 X-ray diffractometer.

The testing of microstructure layers in the TBC was conducted with a Berkovitz's indenter and Nano Scratch-Tester (CSM Instruments).

The examination of cohesion and adhesion of the TBC was carried out with the Revetest Scratch Tester CSM Instruments tool. The surface of sample with the TBC was scratched with the diamond Rockwell's intender of a 200-μm top radius. During the test, six different forces were applied: 2, 4, 8, 16, 32, and 40 N onto the surface of a cross section (MAR-M509 mould and TBC). It has been assumed that each scratch is 0.5 mm long. In the interlayer of the TBC and in the MAR-M509 mould, scratches were made at a 5-N intender load along 0.5 mm. All scratches were made at a rate of 1 mm/min—the speed of the intender. The Revetest Scratch Tester tool was calibrated according to reference sample covered with TiN coating. Friction force, friction factor, and acoustic emission were recorded during the test; 100% of acoustic emission scale equals 65-dB value.

3. Results

3.1. Geometrical structure of a surface

The geometrical product specification (GPS) and the surface load–capacity curve of external ceramic layer in the TBC are presented in Figure 4.

3.2. Microstructure and X-ray diffraction pattern

The microstructure of the plate casting made of alloy MAR-M509 with the TBC at the cross section is presented in Figures 5 and 6. The X-ray diffraction patterns of the external ceramic layer in the TBC surface are shown in Figure 7.

3.3. Measurements of microhardness

Nano Scratch Tester (CSM Instruments) equipped with a Berkovitz's indenter (a pyramid with equilateral triangle as the base area) is to measure microhardness and to determine other mechanical properties of single grains, thin layer, and phase boundaries when loading spreads from 0 to 500 mN [26].

A ratio of elastic strain energy (Ee) to total energy (Ec) when forcing the indenter of the hardness tester is a very important feature of the tested materials.

Figure 8 shows example courses of changes of energy plastic deformation (Ep) and energy of elastic deformation (Ee), which describe the forcing of Berkovitz's indenter into a γ phase, into the metallic interlayer (45% Ni–22% Co–17% Cr–16% Al–0.3% Y), and into the external ceramic layer (ZrO_2) [27]. Table 1 shows values of energy of plastic deformation (Ep), energy of elastic deformation (Ee), total energy (Ec), ratio Ee/Ec, longitudinal modulus of elasticity (Young's modulus E), and microhardness HV0.05 for γ phase, metallic interlayer, and external ceramic layer (the average value from five measurements).

http://dx.doi.org/10.5772/61100

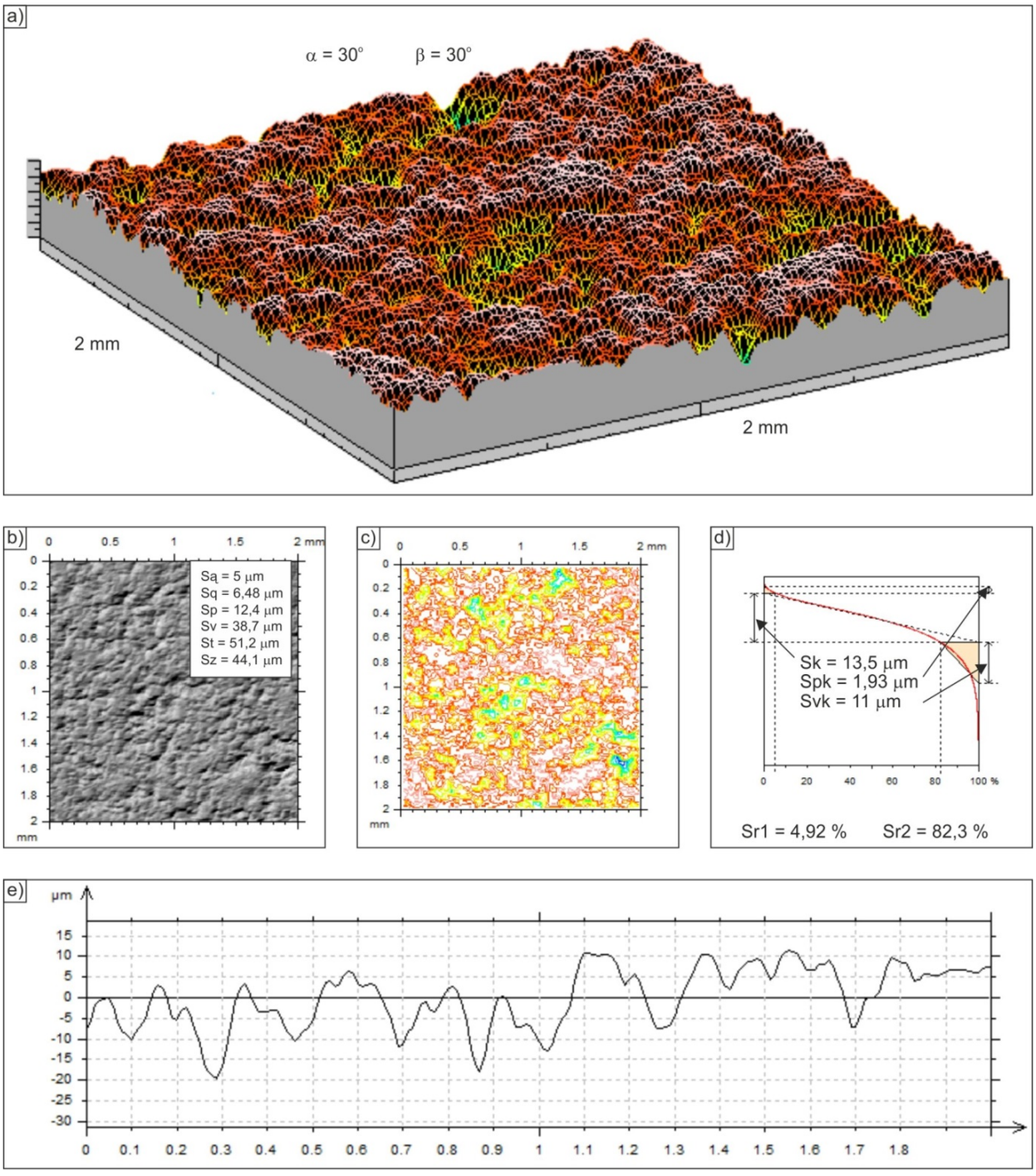

Figure 4. Surface topography of the external ceramic layer in the TBC. 3D view (a), plate surface with amplitude parameters (b), coating map (c), load-capacity curve of GPS and its parameters (d), surface profile (e), and geometrical parameters S_k, S_{pk}, S_{vk}, S_{r1}, S_{r2}.

3.4. Cohesion and adhesion

The control was scratched with the diamond Rockwell's indenter on the surface of a cross-sectional MAR-M509 mould and TBC (Fig. 9).

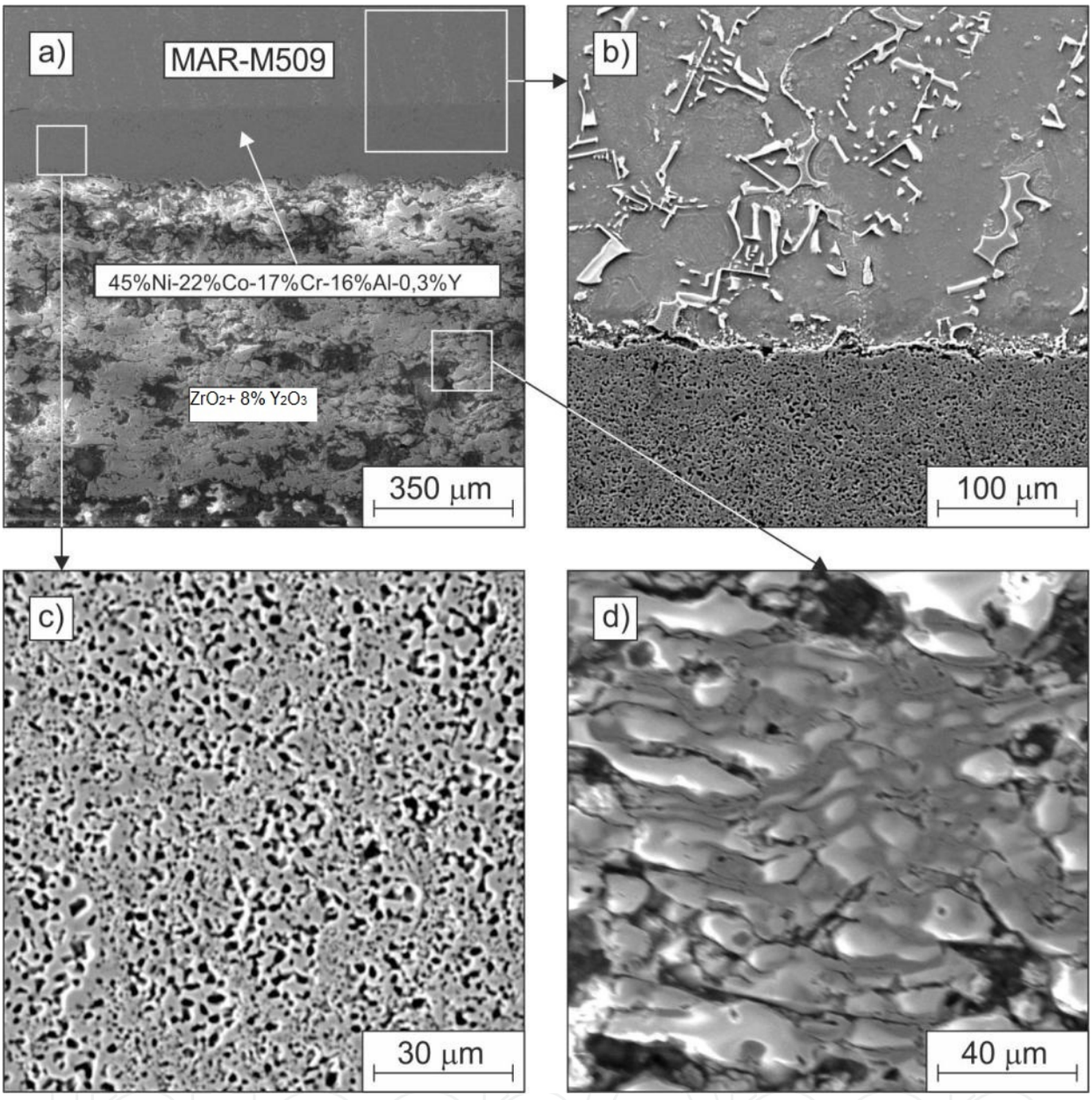

Figure 5. Microstructure at the cross section: mould (MAR-M509) coating (TBC) (a, b), external ceramic layer (ZrO_2) (d), metallic interlayer (45% Ni–22% Co–17% Cr–16% Al–0.3% Y) (c), and SEM micrograph.

Figure 10 shows the surface scratches at the cross section: mould (MAR-M509)–metallic interlayer 45% Ni–22% Co–17% Cr–16% Al–0.3% Y in the TBC together with diagrams of friction force, friction factor, and acoustic emission changes.

The scratches of samples in the direction from the mould (MAR-M509 cobalt alloy) through the metallic interlayer in the TBC at the cross section, which is made at constant intender loads, reveal the presence of typical plastic strain cones (Fig. 10b), crack cones in the coating (Fig. 10a), and "pushes-P" of mould material into this interlayer. The surfaces of longitudinal sections of A_{ca} cones, which characterize the cohesion of the interlayer, are described by a

http://dx.doi.org/10.5772/61100

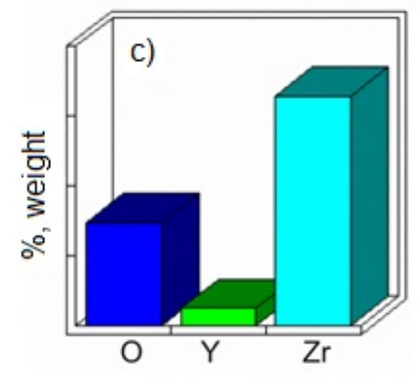

Chemical composition, wt %							
Microarea	O	Al	Cr	Co	Ni	Y	Zr
1	32,04					5,54	62,42
2	32,05						67,95
3		11,74	18,35	21,97	47,94		
4	29,42					4,78	65,80

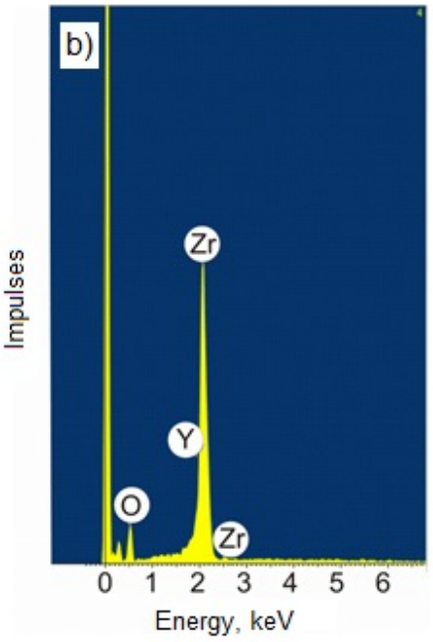

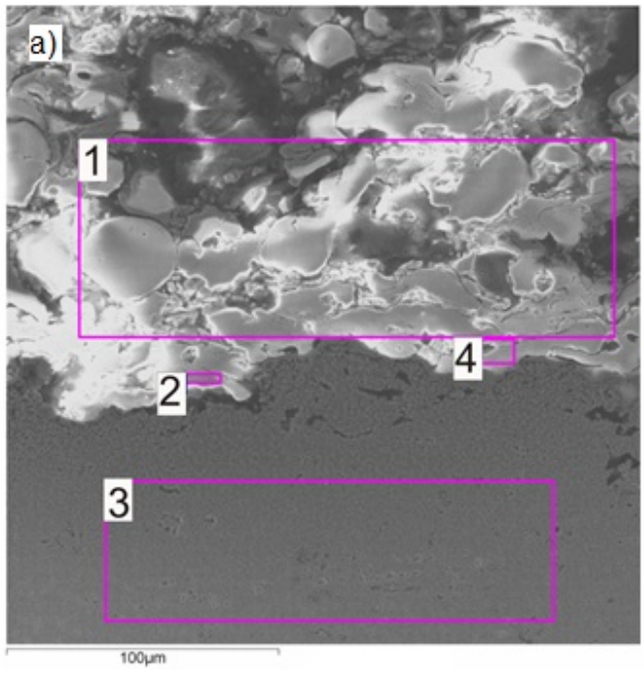

Figure 6. Microstructure of TBC (a), graph of roentgen dispersion radiation from 1 area (b), share of elements in 1 area (c), chemical composition in microareas (1–4) of TBC (table).

product $l_x l_y$ (Fig. 10e) [28] and are plotted as a function of loading force (Fig. 11). The "pushes" of mould material into a metallic interlayer and the lack of cracks at a boundary–mould interlayer (Fig. 11) indicate a very good interlayer adhesion to the mould.

4. Summary

A TBC with ca. 920 μm thickness was obtained as a result of spraying melted powder with particle granulation ca. 75 ± 15 μm made of 45% Ni–22% Co–17% Cr–16% Al–0.3% Y alloy and ceramic powder made of ZrO_2–8% Y_2O_3 oxides with particle irregular granulation ca. 53 ± 15 μm. The surface of a plate casting was made of the MAR-M509 cobalt alloy in a plasma beam (Figs. 5 and 6). Such a coating consists of two layers of fine grain metallic interlayer 45% Ni–

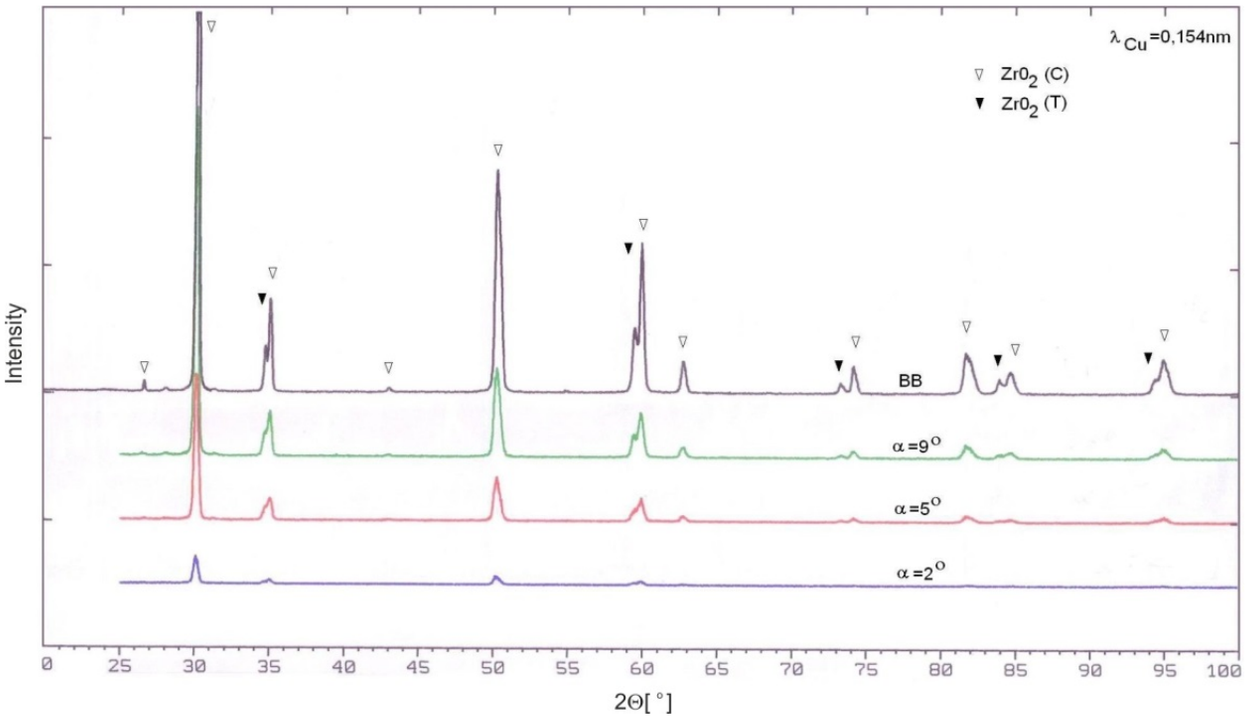

Figure 7. Diffraction patterns of the external ceramic layer in the TBC surface obtained for a grazing incident geometry α = 2°, 5°, and 9° and in the Bragg–Brentano geometry (BB). ZrO_2 (C)—regular, ZrO_2 (T)—tetragonal.

Phase	Ep, pJ	Ee, pJ	Ec, pJ	M_{IT} = Ee/Ec	E, GPa	HV0.05
γ	226739 ± 3%	94733 ± 3%	321458 ± 3%	0.29 ± 0.1	122 ± 5	425 ± 5
Metallic interlayer (45% Ni–22% Co–17% Cr–16% Al–0.3% Y)	257307 ± 5%	72309 ± 3%	333381 ± 5%	0.22 ± 0.1	103 ± 7	540 ± 8
Ceramic external layer (ZrO_2)	16187 ± 5%	16124 ± 5%	32311 ± 5%	0.5 ± 0.1	125 ± 16	1220 ± 45

Table 1. The values of energy of plastic deformation (Ep), energy of elastic deformation (Ee), total energy (Ec), ratio Ee/Ec, Young's modulus E, and microhardness HV0.05. The average value from five measurements.

22% Co–17% Cr–16% Al–0.3% Y (ca. 200 μm thickness) and external ceramic layer as a mixture of two phases, regular ZrO_2 (C) and tetragonal ZrO_2 (T) (Fig. 7). The microstructure of the metallic interlayer in the TBC is tough, homogeneous, and deprived of porosity (total porosity less than 2%) (Fig. 5c). The thin layer of the γ phase (about 0.015 μm thick), which adheres to the metallic interlayer, is characterized by similar values of microhardness as the metallic interlayer, ca. 520 HV0.05. This is an effect of hardening of the γ phase with secondary carbides of $M_{23}C_6$ [27].

http://dx.doi.org/10.5772/61100

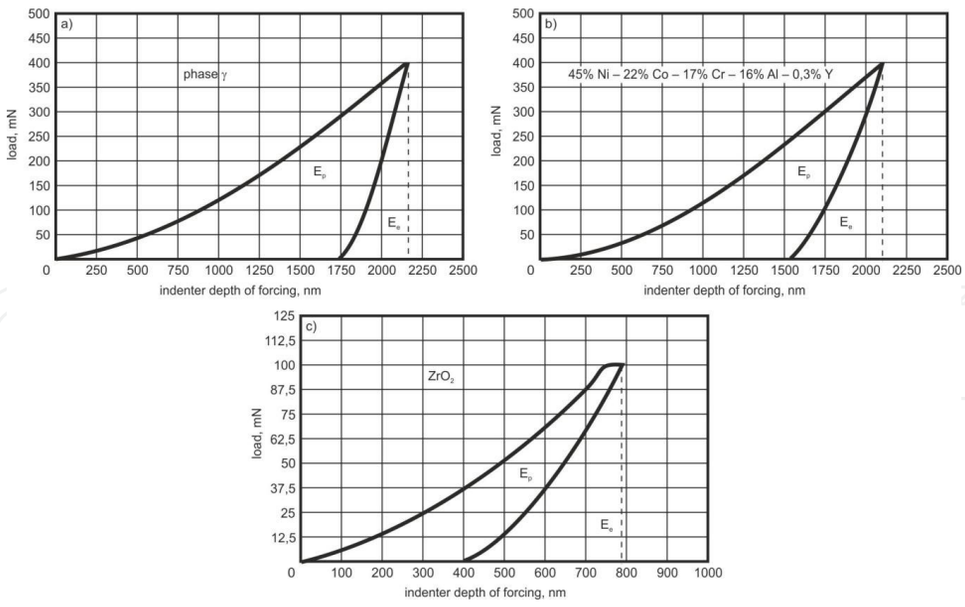

Figure 8. The influence of loading on depth of forcing in the Berkovitz's indenter and energy change for γ phase (a), metallic interlayer (45% Ni–22% Co–17% Cr–16% Al–0.3% Y) (b), and external ceramic layer (ZrO_2) (c).

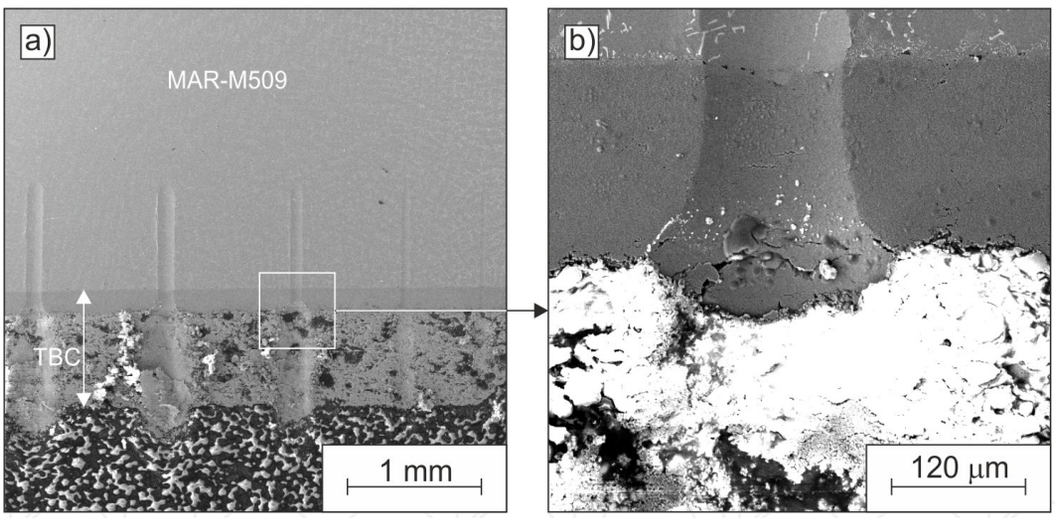

Figure 9. Macrostructure with the picture of surface scratches (a), example of the scratch Rockwell's indenter for the a loading force 8 N of a cross section; MAR-M509 mould, metallic interlayer (45% Ni–22% Co–17% Cr–16% Al–0.3% Y) and external ceramic layer (ZrO_2–8% Y_2O_3) (b), SEM micrograph.

A gradient of elastic strain energy to total energy (M_{IT} = Ee/Ec) when forcing the Berkovitz's indenter is a very good parameter that describes elastic–plastic properties of materials (Fig. 8, Table 1). The M_{IT} parameter equals 0.29 for the γ phase ($M_{IT\gamma}$), 0.22 for the metallic interlayer (M_{ITM}) 45% Ni–22% Co–17% Cr–16% Al–0.3% Y, and 0.50 for the external ceramic layer (MIT_{ZrO2}) (Fig. 12). The metallic interlayer, which has better plastic than the substratum γ phase, was deposited on the plate surface, which was activated by sandblasting with Al_2O_3 particles and by heating at about 120°C. The geometrical product specification (GPS) of the sandblasted plate is isotropic. Its amplitude parameters S_a, S_q, S_p, S_v, S_t, and S_z are 3.1 μm, 3.9 μm, 16.2 μm,

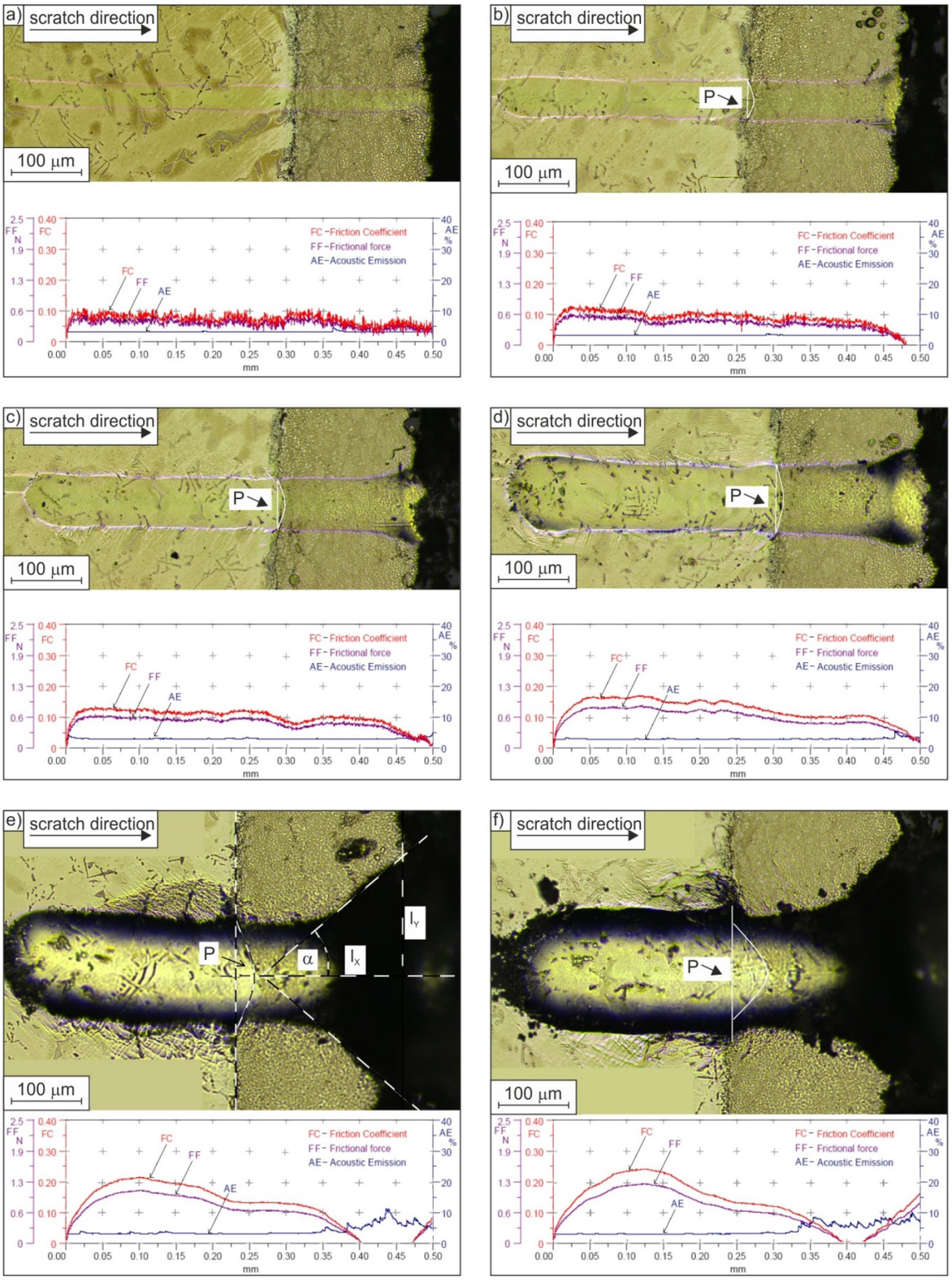

Figure 10. Examples of scratches along the cross section: mould (MAR-M509) interlayer (45% Ni–22% Co–17% Cr–16% Al–0.3% Y) in the TBC, together with diagrams of friction force, friction coefficient, and acoustic emission changes for a loading force2 N (a), 4 N (b), 8 N (c), 16 N (d), 32 N (e), and 40 N (f).

http://dx.doi.org/10.5772/61100

18.3 μm, 34.5 μm, and 31.4 μm, respectively, and functional parameters S_k, S_{pk}, S_{vk}, S_{r1}, and S_{r2} are 10 μm, 4.0 μm, 3.5 μm, 9.6%, and 91.4%, respectively. The GPS of the external ceramic layer in the TBC is also isotropic, but it is rougher than the mould. The total height S_t of the layer has increased by ca. 50%, and the arithmetic mean S_a increased by ca. 60% in comparison to S_t and S_a for the sandblasted surface of the mould. The roughness of the core (S_k) has increased by ca. 35%. The only functional parameter of GPS of ceramic layer, which is lower by ca. 100% in comparison to the mould, is the roughness of peaks (S_{pk}) (Fig. 4).

The scratches of samples along the cross section from the mould (MAR-M509 cobalt alloy) through the metallic interlayer and external ceramic layer (Fig. 9a,b) in the TBC, which were made with Rockwell's cone at different intender loads (Fig. 10a,f), reveal the presence of typical strain and crack cones in the interlayer and "pushes-P" of mould material (γ phase) into the interlayer. A linear surface increase of longitudinal sections of these cones indicates good cohesion of the metallic interlayer (Fig. 11).

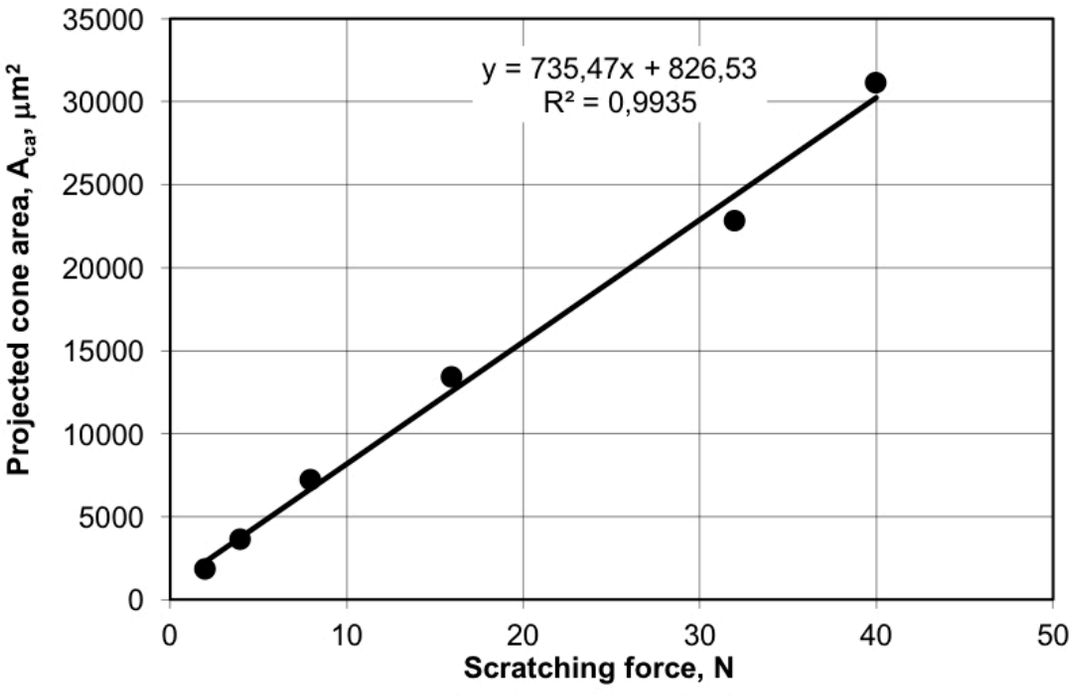

Figure 11. Surfaces of longitudinal sections of A_{ca} cones plotted as a function of loading force in the metallic interlayer 45% Ni–22% Co–17% Cr–16% Al–0.3Y.

A load increase of the Rockwell's intender from 2 N to 40 N (Fig. 10a–f) causes an increase of friction force from ca. 0.3 N to 10 N, together with a minor increase of friction coefficient from ca. 0.1 to 0.2. For all scratches, no increase of acoustic emission effect is observed at boundary mould coating. The constant value of acoustic emission at 3% level (ca. 2 dB) shows that strains at boundary MAR-M509 cobalt alloy–metallic interlayer in the TBC are plastic and do not appear in this crack area (Fig. 10 a–c). The shape of "pushes" of the γ phase is similar to the

cones, and its depth increases linearly together with the increase of intender loading force from ca. 3 μm for 2 N force to ca. 53 μm for 40 N force (Fig. 11). Such a course of changes happening at boundary mould (MAR-M509 cobalt alloy), that is, the metallic interlayer in the TBC during an attempt at scratching, proves a very good adhesion for this interlayer made of 45% Ni–22% Co–17% Cr–16% Al–0.3% Y alloy [29].

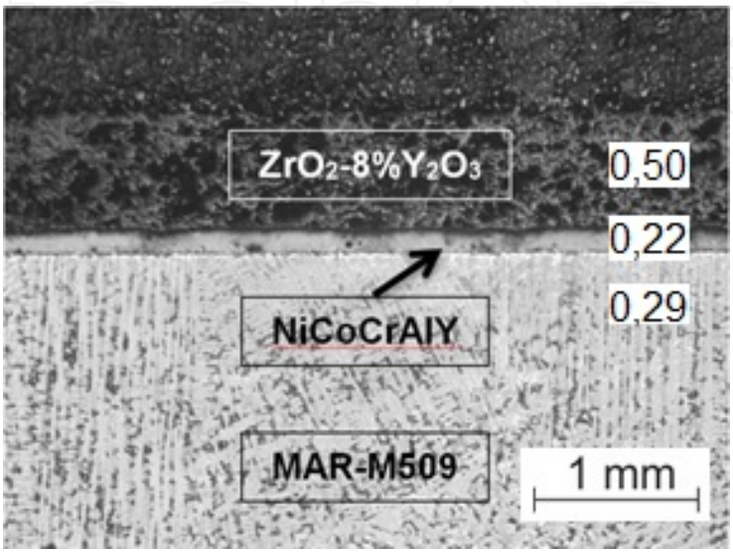

Figure 12. Macrostructure at the cross section: mould (MAR-M509) coating (TBC) with M_{IT} parameters.

Cracks in "cohesion cones" of the metallic interlayer in the TBC are noticed when the loading force of the intender exceeds 16 N (Fig. 10d). Huge differences (even 6.5 dB) between values of acoustic emission are the effect of the interlayer cracking [29] (Fig. 10e,f).

Author details

Zenon Aleksander Opiekun

Address all correspondence to: zopiekun@gmail.com

Department of Casting and Welding, Rzeszów University of Technology, Rzeszów, Poland

References

[1] Pint B.A., Wright J.G., Bridlley W.J.: Evaluation of TBC systems on novel substrates. Journal of Thermal Spray Technology, 9 (6) (2000), 198–203.

[2] Parks W.P. Jr, Hoffman E.E., Lee W.Y. Wright J.G.: Thermal barrier coatings issue in advanced land-based turbines. Journal of Thermal Spray Technology, 6 (2) (1997), 187–192.

[3] Pint B.A., Wright I.G., Lee W.Y., Zhang Y., Prussner K., Aleksander K.B.: Substrate and bond coat compositions. Factory affecting alumina scale adhesion. Materials Science Engineering, A245 (1998), 201–211.

[4] Davis J.R.: Handbook of thermal spray technology ASM. International Materials Park, 2004.

[5] Gugel E., Woetting G.G.: Materials selection for ceramic components in automobiles. Industrial Ceramics, 19 (1999), 196–199.

[6] Masayuki Arai: Damage assessment of tbc sprayed combustor of land-based gas turbine. Journal of the Society of Materials Science, Japan, 57, (3) (2008), 285–291.

[7] Jordan E.H., Gell M.: Solution precursor plasma spray of thermal barrier coatings. Advanced coatings for high temperatures. Processing Turbine Forum, Nicea, 2008.

[8] Stover D., Funke C.: Direction of the development of thermal barrier coatings in energy applications. Journal of Material Processing Technology, (92–93) (1999), 152–202.

[9] Stecura S., Two-layer thermal barrier coatings for high temperature components. Ceramic Bulletin, 56 (1998), 1082–1085.

[10] Coderet Y.: Development of high temperature coatings and TBC bond coats for gas turbine engines. Advanced coatings for high temperatures. Processing Turbine Forum, Nicea, 2008.

[11] Ballard D.J., Schadler L.S., Levis C., Devenport J.: Phase transformation in thermal barrier coatings. Rensselaer Polytechnic Institute Research Experience for Undergraduates, 2000.

[12] Bach W.F., Babiak Z., Duda T., Copitzky T., Josefiak L.A.: Thermal barrier coatings with enhanced properties—a chance for thermal spraying. United Thermal Spray Conference, Dusseldorf, 1999.

[13] Miller A.R.: Thermal barrier coatings for aircraft engines. History and directions. Journal of Thermal Spray Technology (6) (1997), 3.

[14] Haberko K., Pampuch R.: Influence of yttrium content on phase composition and mechanical properties of Y-TZP. Ceramics International (9) (1983), 8–12.

[15] Viancenzini P.: Zirconia thermal barrier coatings for engine application. Industrial Ceramics (10) (1990) 3, 113–126.

[16] Singhal S.C., Bratton R.J.: Stability of a ZrO_2 (Y_2O_3) thermal barrier coating in turbine fuel with contaminants. Transactions of the ASME, 102 (1980), 770–775.

[17] Teixeira Vasco: Numerical analysis of the influence of coating porosity and substrate elastic properties on the residual stresses in high temperature graded coatings. Surface and Coatings Technology, 146–147 (2001), 79–84.

[18] Khor K.A., Gu Y.W.: Effects of residual stress on the performance of plasma sprayed functionally graded ZrO_2/NiCoCrAlY coatings. Materials Science and Engineering, A277 (2000), 64–76.

[19] Guo H.B., Vaßen R., Stöver D.: Thermophysical properties and thermal cycling behavior of plasma sprayed thick thermal barrier coatings. Surface and Coatings Technology, 192 (2005), 48–56.

[20] Vaßen R., Kerkhoff G., Stöver D.: Development of a micromechanical life prediction model for plasma sprayed thermal barrier coatings. Materials Science and Engineering, A303 (2001), 100–109.

[21] Ahmet P., Ozkan S., Erdal C.: Effects of porosity on thermal loadings of functionally graded Y_2O_3-Zr_2O/NiCoCrAlY coatings. Materials and Design, 23 (2002), 641–644.

[22] Traeger F., Ahrens M., Vaßen R., Stöver D.: A life time model for ceramic thermal barrier coatings. Materials Science and Engineering, A358 (2003), 255–265.

[23] Mesratia N., Saif Q., Treheuxb D., Moughilc A., Fantozzic G., Vincent A.: Characterization of thermal fatigue damage of thermal barrier produced by atmospheric plasma spraying. Surface and Coatings Technology, 187 (2004), 185–193.

[24] Opiekun Z.: Analysis of process-related factors that determine structure and properties of cobalt casting alloy intended of aircraft part. Monograph, Poznań, 2007.

[25] Opiekun Z.: Temperature influence of ceramic form on the structure of cobalt alloy MAR-M509 castings. Acta Metallurgica Sinica (English Letters), 24 (1) (2011), 23–33.

[26] ISO 14577 Metallic Materials—Instrumented Indentation Test for Hardness and Material Parameters.

[27] Opiekun Z., Pająk D.: Microstructure and hardness of thermal barrier coating deposited on a high resistant cobalt casting alloy. Rudy iMetaleNieżelazne, 6 (2012), 374–377.

[28] CSM Instruments, Application Bulletin: Characterization of Thermal Spray Instrumented Indentation and Scratch Testing. Part I, No. 28, 2009.

[29] Opiekun Z.A., Trytek A.: Cohesion and adhesion interlayer of the thermal barrier coatings made of cobalt alloy MAR-M509. Archives of Foundry Engineering, 14 (1/2014), 159–164.